REPORT DOCUMENTATION PAGE

Form Approved OMB NO. 0704-0188

1. REPORT DATE (DD-MM-YYYY)	2. REPORT TYPE	3. DATES COVERED (From - To)
03-10-2016	Final Report	1-Jun-2015 - 30-Apr-2016

4. TITLE AND SUBTITLE
Final Report: Unsteady Aerodynamics - Synchronized Flow Control of Dynamic Stall under Coupled Pitch and Freestream

5a. CONTRACT NUMBER: W911NF-15-1-0207

5b. GRANT NUMBER:

5c. PROGRAM ELEMENT NUMBER: 611102

5d. PROJECT NUMBER:

5e. TASK NUMBER:

5f. WORK UNIT NUMBER:

6. AUTHORS
Jeffrey P. Bons, James W. Gregory

7. PERFORMING ORGANIZATION NAMES AND ADDRESSES
Ohio State University
1960 Kenny Road

Columbus, OH 43210 -1016

8. PERFORMING ORGANIZATION REPORT NUMBER

9. SPONSORING/MONITORING AGENCY NAME(S) AND ADDRESS (ES)
U.S. Army Research Office
P.O. Box 12211
Research Triangle Park, NC 27709-2211

10. SPONSOR/MONITOR'S ACRONYM(S)
ARO

11. SPONSOR/MONITOR'S REPORT NUMBER(S)
67417-EG-II.1

12. DISTRIBUTION AVAILIBILITY STATEMENT
Approved for Public Release; Distribution Unlimited

13. SUPPLEMENTARY NOTES
The views, opinions and/or findings contained in this report are those of the author(s) and should not contrued as an official Department of the Army position, policy or decision, unless so designated by other documentation.

14. ABSTRACT
This work presents results of an experimental investigation into synchronized active flow control of a Sikorsky SSC-A09 airfoil undergoing periodic pitching motion in an unsteady free stream using leading edge blowing. The airfoil was evaluated at reduced pitching frequencies up to k=0.05 at steady Mach numbers of 0.2 and 0.4, and at k=0.025 with phase-locked pitch and Mach oscillations at Mach 0.4?0.07 at Reynolds numbers from 1.5 to 3 million. A spanwise row of vortex generator jets (VGJs) located at 10% chord is fed by an oscillating valve that is

15. SUBJECT TERMS
Helicopter Rotor Dynamic Stall, Unsteady Flow Control

16. SECURITY CLASSIFICATION OF: a. REPORT	b. ABSTRACT	c. THIS PAGE	17. LIMITATION OF ABSTRACT	15. NUMBER OF PAGES	19a. NAME OF RESPONSIBLE PERSON
UU	UU	UU	UU		Jeffrey Bons
					19b. TELEPHONE NUMBER: 614-247-8414

Report Title

Final Report: Unsteady Aerodynamics - Synchronized Flow Control of Dynamic Stall under Coupled Pitch and Freestream

ABSTRACT

This work presents results of an experimental investigation into synchronized active flow control of a Sikorsky SSC-A09 airfoil undergoing periodic pitching motion in an unsteady free stream using leading edge blowing. The airfoil was evaluated at reduced pitching frequencies up to k=0.05 at steady Mach numbers of 0.2 and 0.4, and at k=0.025 with phase-locked pitch and Mach oscillations at Mach 0.4?0.07 at Reynolds numbers from 1.5 to 3 million. A spanwise row of vortex generator jets (VGJs) located at 10% chord is fed by an oscillating valve that is phase-locked to the pitch oscillation of the airfoil. The phase and duration of the peak jet mass flux were varied to optimize the flow control benefits to both CL and CM hysteresis loops and reduce negative damping. Peak performance was observed with actuation initiated just after lift stall and continuing for 11% of the pitch cycle. Blowing beyond 11% resulted in no perceptible benefit. Compared to steady blowing flow control, the 11% synchronized control case delivers comparable (or better) performance with less than 50% of the massflow. The degree of stall control is a function of reduced frequency, mass flux ratio, and Mach number.

Enter List of papers submitted or published that acknowledge ARO support from the start of the project to the date of this printing. List the papers, including journal references, in the following categories:

(a) Papers published in peer-reviewed journals (N/A for none)

Received Paper

TOTAL:

Number of Papers published in peer-reviewed journals:

(b) Papers published in non-peer-reviewed journals (N/A for none)

Received Paper

TOTAL:

Number of Papers published in non peer-reviewed journals:

(c) Presentations

An abstract has been submitted to the 2017 AHS conference in Fort Worth Texas in May, 2017. It has not yet been accepted, so it has not been uploaded.

Number of Presentations: 0.00

Non Peer-Reviewed Conference Proceeding publications (other than abstracts):

Received Paper

TOTAL:

Number of Non Peer-Reviewed Conference Proceeding publications (other than abstracts):

Peer-Reviewed Conference Proceeding publications (other than abstracts):

Received Paper

TOTAL:

Number of Peer-Reviewed Conference Proceeding publications (other than abstracts):

(d) Manuscripts

Received Paper

TOTAL:

Number of Manuscripts:

Books

Received Book

TOTAL:

Received	Book Chapter

TOTAL:

Patents Submitted

Patents Awarded

Awards

None

Graduate Students

NAME	PERCENT_SUPPORTED	Discipline
Matthew Frankhouser	0.50	
FTE Equivalent:	**0.50**	
Total Number:	**1**	

Names of Post Doctorates

NAME	PERCENT_SUPPORTED
FTE Equivalent:	
Total Number:	

Names of Faculty Supported

NAME	PERCENT_SUPPORTED	National Academy Member
Jeffrey Bons	0.00	
James Gregory	0.00	
FTE Equivalent:	**0.00**	
Total Number:	**2**	

Names of Under Graduate students supported

NAME	PERCENT_SUPPORTED	Discipline
Rodrigo Auza-Gutierrez	0.10	BS in Aerospace Engineering
FTE Equivalent:	**0.10**	
Total Number:	**1**	

Student Metrics

This section only applies to graduating undergraduates supported by this agreement in this reporting period

The number of undergraduates funded by this agreement who graduated during this period: 1.00

The number of undergraduates funded by this agreement who graduated during this period with a degree in science, mathematics, engineering, or technology fields:...... 1.00

The number of undergraduates funded by your agreement who graduated during this period and will continue to pursue a graduate or Ph.D. degree in science, mathematics, engineering, or technology fields:...... 1.00

Number of graduating undergraduates who achieved a 3.5 GPA to 4.0 (4.0 max scale):...... 1.00

Number of graduating undergraduates funded by a DoD funded Center of Excellence grant for Education, Research and Engineering:...... 0.00

The number of undergraduates funded by your agreement who graduated during this period and intend to work for the Department of Defense 0.00

The number of undergraduates funded by your agreement who graduated during this period and will receive scholarships or fellowships for further studies in science, mathematics, engineering or technology fields:...... 1.00

Names of Personnel receiving masters degrees

NAME	
Matthew Frankhouser	
Total Number:	**1**

Names of personnel receiving PHDs

NAME
Total Number:

Names of other research staff

NAME	PERCENT_SUPPORTED
FTE Equivalent:	
Total Number:	

Sub Contractors (DD882)

Inventions (DD882)

Scientific Progress

I have attached a 13 page report that documents the study in great detail. Sections in the report include: Introduction, Experimental Facility, Results, and Conclusions. It would be impossible for me to adequately summarize the work in this short block without being able to import the figures and tables. Please refer to the attachment.

Technology Transfer

Presented findings at ARO contractors meeting in July, 2016.
Discussed preliminary findings with relevant parties at AHS 2016 in Palm Springs, FL.

SECTION	PAGE NUMBER
Table of Contents	**1**
DD Form882	**2**
Project Abstract	**3**
Project Final Report	**4-15**
Bibliography	**16**

REPORT OF INVENTIONS AND SUBCONTRACTS

(Pursuant to "Patent Rights" Contract Clause) (See Instructions on back)

Form Approved
OMB No. 9000-0095
Expires Jan 31, 2008

PLEASE DO NOT RETURN YOUR COMPLETED FORM TO THE ABOVE ORGANIZATION. RETURN COMPLETED FORM TO THE CONTRACTING OFFICER.

1.a. NAME OF CONTRACTOR/SUBCONTRACTOR	c. CONTRACT NUMBER	2.a. NAME OF GOVERNMENT PRIME CONTRACTOR	c. CONTRACT NUMBER	3. TYPE OF REPORT (X one)
Ohio State University	W911NF-15-1-0207	same	W911NF-15-1-0207	a. INTERIM [ ] b. FINAL [X]
b. ADDRESS (Include ZIP Code) 2300 West Case Rd Columbus, OH 43235	d. AWARD DATE (YYYYMMDD) 20150430	b. ADDRESS (Include ZIP Code) same	d. AWARD DATE (YYYYMMDD) 20150430	4. REPORTING PERIOD (YYYYMMDD) a. FROM 20150801 b. TO 20160430

SECTION I - SUBJECT INVENTIONS

5. "SUBJECT INVENTIONS" REQUIRED TO BE REPORTED BY CONTRACTOR/SUBCONTRACTOR (If "None," so state)

NAME(S) OF INVENTOR(S) (Last, First, Middle Initial) a.	TITLE OF INVENTION(S) b.	DISCLOSURE NUMBER, PATENT APPLICATION SERIAL NUMBER OR PATENT NUMBER c.	d. ELECTION TO FILE PATENT APPLICATIONS (X) (1) UNITED STATES (a) YES	(1) UNITED STATES (b) NO	(2) FOREIGN (a) YES	(2) FOREIGN (b) NO	e. CONFIRMATORY INSTRUMENT OR ASSIGNMENT FORWARDED TO CONTRACTING OFFICER (X) (a) YES	(b) NO
	none							

f. EMPLOYER OF INVENTOR(S) NOT EMPLOYED BY CONTRACTOR/SUBCONTRACTOR

(1) (a) NAME OF INVENTOR (Last, First, Middle Initial)

(b) NAME OF EMPLOYER

(c) ADDRESS OF EMPLOYER (Include ZIP Code)

(2) (a) NAME OF INVENTOR (Last, First, Middle Initial)

(b) NAME OF EMPLOYER

(c) ADDRESS OF EMPLOYER (Include ZIP Code)

g. ELECTED FOREIGN COUNTRIES IN WHICH A PATENT APPLICATION WILL BE FILED

(1) TITLE OF INVENTION

(2) FOREIGN COUNTRIES OF PATENT APPLICATION

SECTION II - SUBCONTRACTS *(Containing a "Patent Rights" clause)*

6. SUBCONTRACTS AWARDED BY CONTRACTOR/SUBCONTRACTOR (If "None," so state)

NAME OF SUBCONTRACTOR(S) a.	ADDRESS (Include ZIP Code) b.	SUBCONTRACT NUMBER(S) c.	d. FAR "PATENT RIGHTS" (1) CLAUSE NUMBER	(2) DATE (YYYYMM)	DESCRIPTION OF WORK TO BE PERFORMED UNDER SUBCONTRACT(S) e.	f. SUBCONTRACT DATES (YYYYMMDD) (1) AWARD	(2) ESTIMATED COMPLETION
none							

SECTION III - CERTIFICATION

7. CERTIFICATION OF REPORT BY CONTRACTOR/SUBCONTRACTOR (Not required if: (X as appropriate)) [ ] SMALL BUSINESS or [ ] NONPROFIT ORGANIZATION

I certify that the reporting party has procedures for prompt identification and timely disclosure of "Subject Inventions," that such procedures have been followed and that all "Subject Inventions" have been reported.

a. NAME OF AUTHORIZED CONTRACTOR/SUBCONTRACTOR OFFICIAL (Last, First, Middle Initial)	b. TITLE	c. SIGNATURE	d. DATE SIGNED
Bons, Jeffrey P	Professor	[signature]	20160930

DD FORM 882, JUL 2005 PREVIOUS EDITION IS OBSOLETE. FormFlow/Adobe Professional 6.0

Title: P1.1.2 Unsteady Aerodynamics - Synchronized Flow Control of Dynamic Stall under Coupled Pitch and Freestream Oscillations

PI: Prof. Jeffrey P. Bons, The Ohio State University
Co-PI: Prof. James W. Gregory, The Ohio State University

Duration: 9 months, Short Term Innovative Research (STIR) **Budget:** $50k

Project Abstract

This work presents results of an experimental investigation into synchronized active flow control of a Sikorsky SSC-A09 airfoil undergoing periodic pitching motion in an unsteady free stream using leading edge blowing. The airfoil was evaluated at reduced pitching frequencies up to k=0.05 at steady Mach numbers of 0.2 and 0.4, and at k=0.025 with phase-locked pitch and Mach oscillations at Mach 0.4±0.07 at Reynolds numbers from 1.5 to 3 million. A spanwise row of vortex generator jets (VGJs) located at 10% chord is fed by an oscillating valve that is phase-locked to the pitch oscillation of the airfoil. The oscillating valve can be set to produce a peak jet mass flux ratio (C_q) of 0.0022 or 0.0028 with a background C_q of half this value over the remainder of the period. The phase and duration of the peak C_q were varied to optimize the flow control benefits to both C_L and C_M hysteresis loops and reduce negative damping. Peak performance was observed with actuation initiated just after lift stall and continuing for 11% of the pitch cycle. Blowing beyond 11% resulted in no perceptible benefit. Compared to steady blowing flow control, the 11% synchronized control case delivers comparable (or better) performance with less than 50% of the massflow. The degree of stall control is a function of reduced frequency, mass flux ratio, and Mach number.

Synchronized Flow Control of Dynamic Stall under Coupled Pitch and Freestream Oscillations

Jeffrey P. Bons
Professor

Matthew W. Frankhouser
Graduate Research Associate

James W. Gregory
Associate Professor

Aerospace Research Center, The Ohio State University, Columbus, Ohio, United States

ABSTRACT

This work presents results of an experimental investigation into synchronized active flow control of a Sikorsky SSC-A09 airfoil undergoing periodic pitching motion in an unsteady free stream using leading edge blowing. The airfoil was evaluated at reduced pitching frequencies up to *k*=0.05 at steady Mach numbers of 0.2 and 0.4, and at k=0.025 with phase-locked pitch and Mach oscillations at Mach 0.4±0.07 at Reynolds numbers from 1.5 to 3 million. A spanwise row of vortex generator jets (VGJs) located at 10% chord is fed by an oscillating valve that is phase-locked to the pitch oscillation of the airfoil. The oscillating valve can be set to produce a peak jet mass flux ratio (C_q) of 0.0022 or 0.0028 with a background C_q of half this value over the remainder of the period. The phase and duration of the peak C_q were varied to optimize the flow control benefits to both C_L and C_M hysteresis loops and reduce negative damping. Peak performance was observed with actuation initiated just after lift stall and continuing for 11% of the pitch cycle. Blowing beyond 11% resulted in no perceptible benefit. Compared to steady blowing flow control, the 11% synchronized control case delivers comparable (or better) performance with less than 50% of the massflow. The degree of stall control is a function of reduced frequency, mass flux ratio, and Mach number.

NOTATION

c	Airfoil chord
C_L	Lift coefficient
C_M	Moment coefficient
C_P	Pressure coefficient, $\frac{P-P_\infty}{\frac{1}{2}\rho_\infty U_\infty^2}$
C_q	Mass Flux Ratio, $\frac{\dot{m}_j}{\rho_\infty U_\infty c L_{act}}$
f	Physical frequency
k	Reduced frequency $\frac{c\pi f}{U_\infty}$
L_{act}	Effective span of VGJs
M	Mach number
$\dot{m}$	Mass flow rate
P	Pressure
U	Velocity
x	Chordwise position
α	Angle of attack
ρ	Density
$\Delta\Phi$	Phase difference between M and α

Subscripts

avg	Average value
init	Jet initiation angle of attack
j	Jet
max	Maximum value
on	Jet on time as a % of pitching cycle
∞	Freestream

INTRODUCTION

Dynamic stall (DS) is a performance-limiting phenomenon experienced by rotorcraft in forward flight and in maneuvers. The lift and moment stall due to the shed vortex can produce significant variations in pitching moment. The transient, very high pitch link loads resulting from dynamic stall force design choices that add to the weight of the vehicle, and limit the operational envelope of the rotorcraft.

Relevant studies of dynamic stall stretch over four decades, such that the basic phenomena of dynamic stall under static freestream conditions are thoroughly documented (McCroskey et al., Ref. 1, and Carr, Ref. 2). Contemporary investigations of the intricate details of dynamic stall are also currently underway (Geissler et al., Ref. 3; Mulleners and Raffel, Ref. 4; Raghav and Komerath, Ref. 5; Pruski and Bowersox, Ref. 6; and Muller-Vahl et al., Ref. 7). Due to large amplitude pitching motions, compressibility effects can be important for onset Mach numbers as low as 0.2. The state of the boundary layer and its susceptibility to separation are in turn functions of Reynolds number. Thus, the two flow parameters are strongly coupled. Typical onset Mach and Reynolds number ranges are 0.2-0.5 and 2-6 million, respectively, for retreating blade stall.

The majority of helicopter rotor dynamic stall studies reported in the literature have been conducted in constant velocity wind tunnels with either a 2D airfoil pitching (or plunging) at the appropriate reduced frequency. In reality, since the rotor stall occurs during the retreating blade motion (at advance ratios approaching 0.3-0.4), the component of the vehicle advance velocity "seen" by the retreating airfoil also varies during the dynamic stall event. Thus, in a rotor-relative frame, both the approach flow angle (due to pitch/plunge) and magnitude are time-varying. This time-varying relative velocity has a direct influence on the severity of the local pressure gradient and thus, the formation of the dynamic stall process as shown by Ericsson (Ref. 8). Several researchers have investigated the combination of airfoil pitching and relative velocity oscillations (Pierce et al., Ref. 9; ; Favier et al., Ref. 10; and Furman et al., Ref. 11) and concluded that a strong coupling exists between the two modes of oscillation. Of note, all of these studies have been conducted at incompressible flow speeds below Mach 0.1. Recently, Hird et al. (Ref. 12) studied the combined effects of fluctuating pitch and freestream velocity at a mean Mach number of 0.4 and at reduced frequencies up to k=0.05 (conditions equivalent to a rotor advance ratio of 0.2). They found that the peak C_{Lmax} was increased well beyond the peak value observed in steady freestream conditions. They also reported a more abrupt lift stall without a significant change in the stall angle. It is anticipated that these differences between steady and unsteady Mach will only be exacerbated at advance ratios closer to those experienced at typical dynamic stall onset (0.3-0.4).

Numerous attempts have been made to implement flow control on a dynamically pitching airfoil and limit the negative effects of dynamic stall. Chandrasekhara et al. (Ref. 13) implemented a dynamically deforming leading edge model (DDLE) that modified the leading edge radius to adapt to high vs. low flow Mach numbers. Though the authors indicated that the DDLE could be operated in dynamic mode, the report only includes static LE deformation. Other passive flow control strategies have also been implemented with some success (LE slat - Carr et al., Ref. 14, variable droop leading edge, Martin et al., Ref. 15, and trailing edge flaps, Gerontakas et al., Ref. 16). Active blowing has also been very effective as demonstrated by Greenblatt and Wygnanski (Ref. 17), Singh et al., (Ref. 18), Gardner et al. (Ref. 19), Naigle et al. (Ref. 20) and Matalanis et al. (Ref. 21). All of these blowing cases have either been steady or pulsed at a frequency much higher than the pitch oscillation frequency (so that phasing or synchronizing the control was not attempted). Though the continuous blowing strategies have shown considerable success at improving mean lift and muting the moment spike, virtually all of the researchers recognized the potential value of synchronizing the fluidic actuation with the pitch oscillation. This would allow the control to only be employed when it is beneficial to the airfoil performance as well as reducing the massflow requirement. Post and Corke (Ref. 22) did synchronize SDBD plasma actuators with the pitch oscillation and showed that this was more effective than continuous actuation through the complete pitch oscillation, though their flow Mach number was 0.03 (incompressible). Moreover, none of these flow control studies have included Mach oscillation.

More recently, Tran et al. (Ref. 23) modeled synchronized blowing from a synthetic jet on a pitching SC1095 airfoil using unsteady RANS. When comparing continuous actuation to partial actuation (for just 30% of the pitching cycle), they found that synchronized partial blowing actually outperformed continuous blowing. Though no optimization of the timing was presented, the jets were actuated at 17° on the upstroke (before lift stall) and terminated at 18.5° on the downstroke (pitch oscillation was from 10 to 20°). Finally, Matalanis et al. (Ref. 24) integrated a row of combustion actuators (COMPACT) into a VR-12 airfoil and varied the starting phase and duration over a wide range of parameters. Experimentally, they showed that actuation for more than 30% of the pitch cycle provided no additional benefit in terms of cycle-averaged lift. Optimum actuation occurred when initiating the F^+=0.4 pulsed forcing following the lift stall and just prior to moment stall. Experiments were run over relevant ranges of Mach number (0.2 to 0.4) and reduced frequency (0.05 < k < 0.1).

The aforementioned flow control studies were all done on oscillating airfoils in a steady freestream. Herein lies the motivation for this study; to expand active flow control using VGJs with synchronized oscillations of both airfoil pitch and freestream Mach number, at reduced frequencies and Reynolds numbers representative of realistic helicopter operating conditions.

EXPERIMENTAL METHODOLOGY

Data collection was conducted in the 6"×22" blowdown transonic wind tunnel at The Ohio State University, the design and capabilities of which are detailed by Gompertz *et al*. (Ref. 25). The tunnel has electrically operated rotating mechanisms to oscillate the airfoil pitch and the freestream Mach number synchronously. Figure 1 is a schematic of the tunnel and Fig. 2 shows the range of possible operating conditions for the tunnel. The freestream flow is supplied to the test section through a 20 cm (8 in.) supply line from two 42.5 m^3 (1500 ft^3) air storage tanks pressurized up to 17 MPa (2500 psi) with in-line air dryers to control condensation. The high pressure air flow is controlled by two valves. The first is a control valve which sets the total pressure. The flow density and Reynolds number for the experiment are established by the total pressure combined with the flow temperature. The second valve is a fast acting valve used to start and stop the flow. The maximum limiting pressure of the wind tunnel is 350 kPa (50 psia). The settling chamber is equipped with a perforated plate, a honeycomb section, and eight screens (60-mesh) to condition the flow and lower the test-section turbulence intensity to less than 0.5% under steady flow conditions. A subsonic nozzle with a contraction ratio of 15:1 further establishes flow uniformity in the 15.2 cm × 55.9 cm test section, which is 1.1 m long. The solid sidewalls have clear and opaque windows to hold the airfoil, while the spanwise floor and ceiling walls are perforated with 3.2-mm straight holes yielding an effective porosity of 6 percent. These isolation cavities are open to the flow only downstream of the test section and aid in producing a high quality flow in the test section by reducing Mach wave reflections in transonic flow.

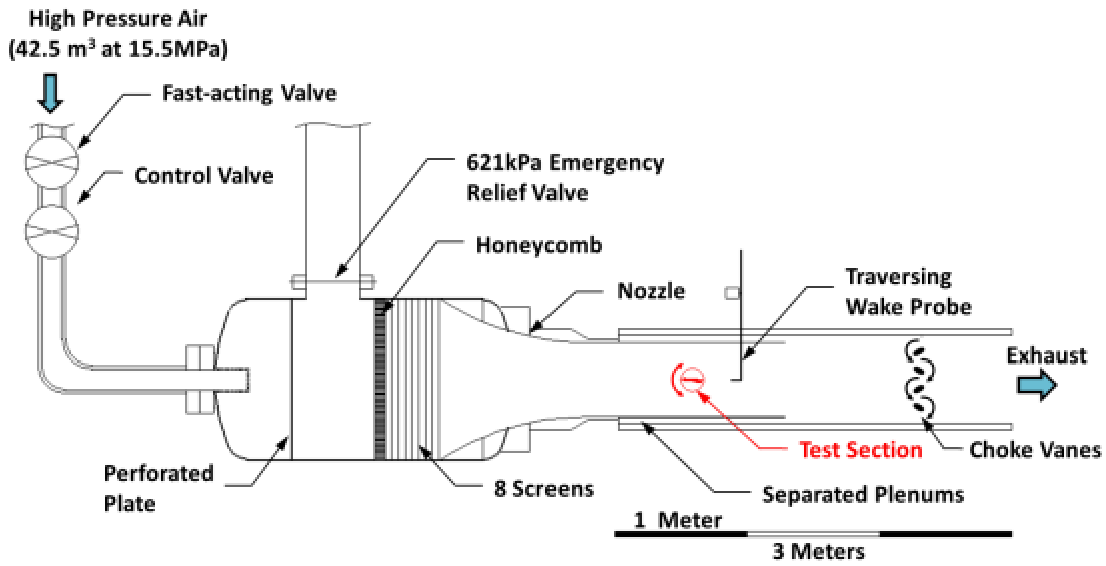

Figure 1: Schematic of the OSU 6"×22" Transonic Blowdown Tunnel.

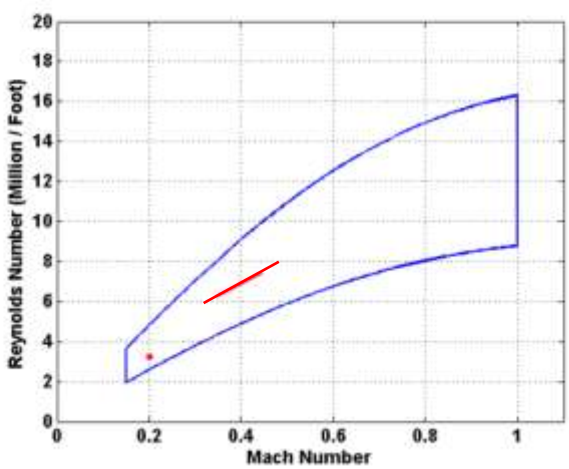

Figure 2: Operating Envelope of 6"×22" Tunnel (Red markings denote operating conditions for this study).

The tunnel is always operated in a choked-flow condition, with the throat downstream of the test section. The throat area can be easily modified for both static and dynamic Mach number by changing the cross-sectional area and shape of evenly-spaced blockage bars that form the throat area. Since the test section Mach number is uniquely established by the ratio of choke area and test section area, Reynolds number can be set independently of the Mach number by controlling stagnation pressure (see Fig. 2). The Mach number will remain isolated from stagnation pressure fluctuations downstream of the choke bars as long as the flow remains choked. Pitch oscillations about the airfoil quarter chord are generated by a cam-driven linkage connected to a 3.7 kW (5hp) motor. This mechanism drives the angle of attack in an approximately sinusoidal waveform at physical frequencies up to 21 Hz.

Mach oscillations are produced by a set of four elliptical choke vanes driven by a stepper motor slaved to the pitch oscillation motor. The choke vane stepper motor is slaved such that the Mach oscillation frequency is synchronized to the pitch oscillation frequency at a desired phase delay through a predetermined phase offset ($\Delta\Phi$). For this study, $\Delta\Phi$ was set to 180°, which is the realistic flow condition for a rotor in forward flight. As the blowdown tunnel is operated at a sufficiently high pressure ratio to choke the flow at the downstream throat, the throat area produced by the choke vanes uniquely modulates the test section Mach number. Gompertz *et al.* (Ref. 25) characterized these details of the wind tunnel and calculated pressure wave propagation through the tunnel. Due to the oscillating frequencies of the elliptical choke vanes and the pressure translation through the tunnel, the resultant Mach amplitude varies slightly at higher reduced frequencies from an ideal sinusoidal pattern of M=0.4±0.07 as depicted in Fig. 3. At low reduced frequencies, the variation in Mach number matches the predicted sinusoid well, but at the highest reduced frequencies, there is some distortion of the waveform as well as a phase lag. However, in all cases, the mean Mach remains at 0.4.

Instrumentation and Test Article

The airfoil used for this study was a milled aluminum SSC-A09 model with span and chord of 15.2 cm (6 in.) resulting in an aspect ratio of 1 (Fig. 4). The model was fitted with 30 pressure taps on the suction surface and 23 taps on the pressure surface. The pressure taps were connected to two ESP 32HD pressure scanners via flexible tubing of 1 mm in diameter and approximately 20 cm long. A hardware-triggered DTC Initium interface read in the multiplexed analog output of the scanners at 1000 Hz and streamed the data to a dedicated hard disk. The scanner

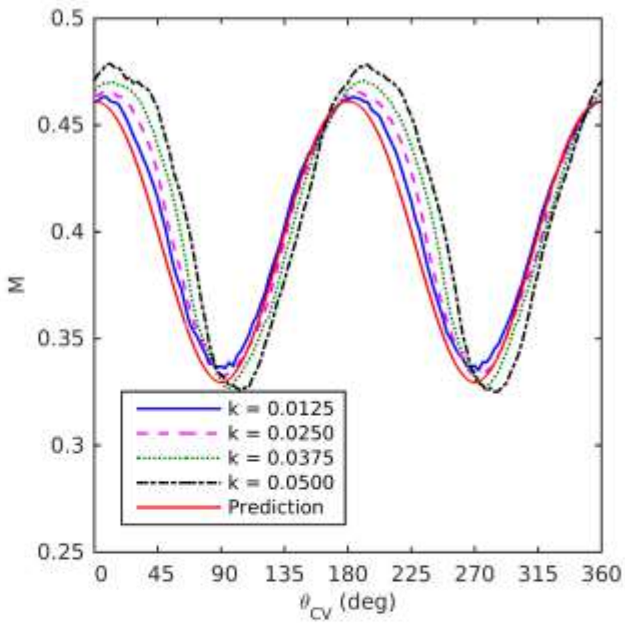

Figure 3: Empty Tunnel Mach Variation with Reduced Frequency.

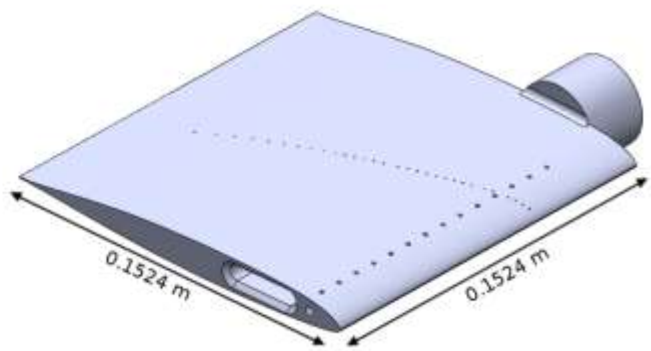

Figure 4: SSC-A09 Airfoil with Spanwise VGJs and Surface Pressure Taps.

system is thermally compensated to minimize zero and span shifts. The pressure scanners were triggered by a TTL pulse train to ensure a harmonized sample interval and accurate temporal correlation with other instrumentation.

Attenuation and delays in measured pressure signals due to viscous effects in the tubing-sensor system were studied in detail prior to taking dynamic pressure measurements. The Bergh and Tijdeman (Ref. 26) model was coupled with dynamic calibration data to develop a compensatory transfer function based on the tubing diameter, length and transducer volume. The resulting transfer function from the empirical data and the fitted model from the experiment are in excellent agreement, providing a suitable scheme for the attenuation and phase compensation of the unsteady pressure data. The analytical / experimental model showed dominant frequencies above 100 Hz. This is above the maximum oscillating frequency (21 Hz) by a factor of 5. Therefore, for the tubing diameter and length used in the experiment, the amplification and phase compensation insignificantly altered the measurements of the unsteady pressures. All results in this paper have been appropriately compensated based on this combined analytical /experimental model.

The airfoil was fabricated with a row of spanwise vortex generating jets near the leading edge. The VGJ diameter and spacing are 1% and 5.6% of airfoil chord, respectively (see Fig. 4). For all of the results in this study, every other hole was filled and sanded smooth creating a new spacing of 11.2% of airfoil chord and spread over the center 10 cm (4 in) of span (L_{act}). The VGJs are located at 10% chord as this was the typical release point for the dynamic stall vortex on the SSC-A09 airfoil, as determined by Lorber and Carta (Ref. 27) at comparable reduced frequencies and Mach number. The VGJs are oriented normal to the surface, which is similar to the configuration determined by Gardner *et al*. (Ref. 19) to be optimal for dynamic stall control at higher maximum angles of attack. An internal uniform cavity with a diameter of 3mm (0.125 in.) at 10% chord served as a VGJ manifold and connected the airfoil to the high pressure air source through a threaded steel tube.

High pressure air was stepped down from greater than 10.3 MPa (1500 psi) to a maximum of 2 MPa (300 psi) before entering the oscillating valve shown in Fig. 5. The valve consists of a cylindrical plenum with an entrance and exit port. The exit port is covered by a circular disk that seals to the plenum walls. The disk is connected to a shaft that enters the plenum through the opposing wall. The shaft, in turn, is connected to a belt pulley that is driven by the same linkage that drives the airfoil pitch oscillation. The disk has a cutout that lines up with the plenum exit port to produce the pulsed jet. Cutouts of 15, 40, and 60 degree width were used to create high pressure pulses of 4.2%, 11.1%, and 16.7% of the pitching period. The initiation of the high pressure release is controlled by adjusting the alignment of the cutout with the exit port. In this study, alignments were chosen to trigger the high pressure pulse just after lift stall (α = 17°, 18°, and 19°), based on the findings of Matalanis et al. (Ref. 24).

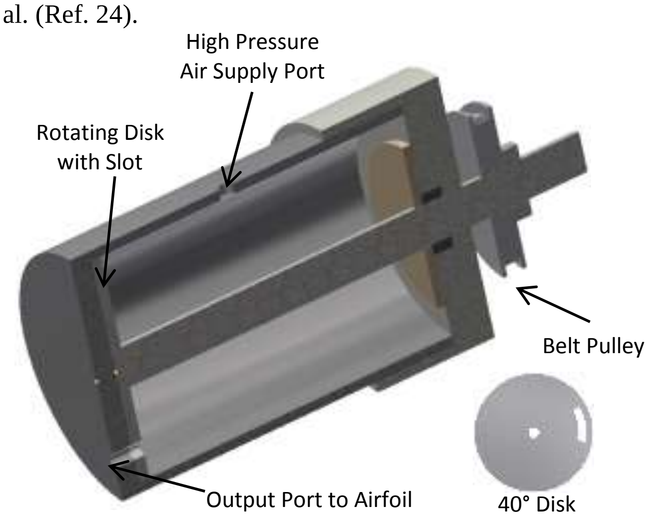

Figure 5: Oscillating valve used for synchronized blowing. 40° disk shown in inset.

A pressure transducer and thermocouple were installed on the piping upstream of the flexible tubing that connects the oscillating valve to the airfoil. The instrumental uncertainty for the pressure gauge and thermocouple are ±5 psig and ±0.1K, respectively. The time history of exiting massflux from the VGJs during unsteady wind tunnel operation was estimated as follows. With the wind tunnel off and steady flow through the VGJs, the massflux was measured with an Alicat MCR Series 3000 SLPM mass flow controller and correlated to the measured pressure difference between the tubing just outside the airfoil to the static pressure at the VGJ exit. This correlation was then used to estimate the massflux during unsteady operation using the same delta pressure measurement with the airfoil pitching in the unsteady freestream. It is acknowledged that during unsteady operation there is likely to be some modulation of the pulse amplitude from the pressure measurement location to the VGJ exit, but this was not accounted for.

The calculation of jet mass flux ratio (C_q) is defined below where $\dot{m}_j$ is the mass flow rate of the jets, ρ_∞ and U_∞ are freestream density and velocity, respectively, and the effective span with VGJs fitted is L_{act}.

$$C_q = \frac{\dot{m}_J}{\rho_\infty U_\infty c L_{act}}$$

Samples of $C_q(\alpha)$ histories are provided in Fig. 6 for the "High" supply pressure and all 3 cutout disks at Mach=0.2 and k=0.05 (the trends are similar for the other cases studied). In this figure, actuation was initiated at α=18°.

As is evident from Fig. 6, the massflux from the VGJs is not uniform over the pulse duration, instead exhibiting a sharp peak immediately following the disk cutout alignment with the output port of the oscillating valve plenum. Due to compressibility of the air in the valve plenum, the flexible tubing, and the airfoil plenum, the sharp peak is followed by a gradual drop as shown. The shape of this drop off varies with the duration of the pulse (4.2%, 11.1%, or 16.7%). The figure also shows that due to leakage around the rotating disk in the plenum, the massflow does not drop to zero, instead holding at some constant value throughout most of the upstroke. To facilitate comparison between synchronized and continuous (steady) actuation, several tests were conducted with constant blowing levels (bypassing the oscillating valve altogether). These steady C_q levels are indicated on Fig. 6 as well. An attempt was made to test at steady blowing values corresponding to the peak jet velocity and a lower value for both operating pressures. These steady comparisons are identified as "Peak" and "Mean" in the plot and will be referred to later. It should be noted that the 11.1% C_q time history differs noticeably from the others at both Low and High pressure settings. This is thought to be due to a better sealing of the 40° disk during rotation.

DATA ANALYSIS

As this is a transient tunnel, the tunnel conditions are constant for a period of 6 seconds during which time surface and tunnel pressure data are acquired at 1000 Hz. The data are analyzed and truncated as necessary to eliminate tunnel acceleration or deceleration transients. The resultant sample for steady data is time-averaged over 4.5 seconds. The unsteady data are phase-averaged over 14 to 56 cycles depending on the pitching frequency with higher frequency associated with more averaged cycles. Calculations for lift and moment coefficients were obtained by trapezoidal integration of the measured pressure distributions.

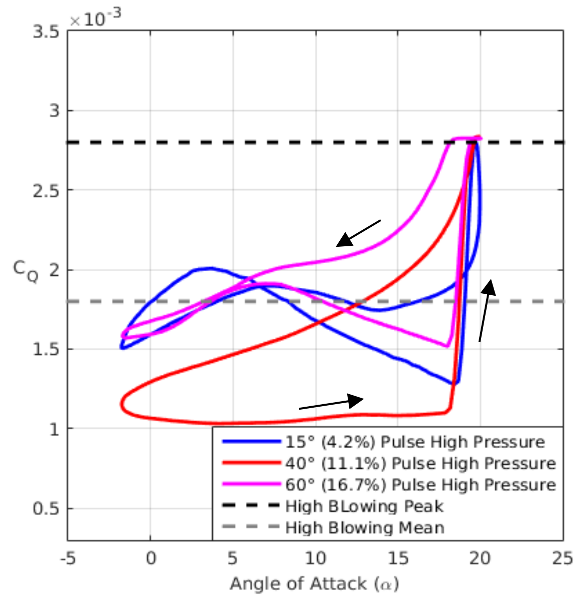

Figure 6: C_q vs. α time history for 15° (4.2%), 40° (11.1%), and 60° (16.7%) cutout disks at Mach=0.2 and k=0.05 for the "High" pressure level. Steady blowing C_q values for peak and mean pressure also indicated. Arrows indicate direction of pitching motion in time.

Temperature, pitch, and Mach phase revolutions were acquired at 100 kHz for 10 seconds such that temperature and phase data overlapped the duration of pressure acquisition. Lift and moment coefficient calculations were synchronized with the corresponding angle of attack (from an optical encoder) to generate lift and moment loops.

An analysis was conducted in the manner outlined by Coleman and Steele (Ref. 28) to estimate the relevant calibration uncertainties with the wind tunnel in steady-flow mode. Gompertz *et al.* (Ref. 25) showed tunnel-relevant dominant uncertainty estimates based on pressure instrumentation to be: Mach number, ±0.005; Reynolds number, ±5,000; angle of attack, ±0.05°; C_P, ±0.05; C_L, ±0.05; and C_M, ±0.02. The uncertainty of the jet mass flux ratio (C_q) is ±0.00005, though this does not account for differences between the pressure measured at the inlet to the VGJ plenum and pressure at the inlet to each VGJ (as discussed above).

RESULTS AND DISCUSSION

Baseline, No Control, Steady Freestream:

Figure 7 show the uncontrolled pitching airfoil c_L and c_M hysteresis loops for the case of steady flow at M=0.2. Results are included for k=0.025 and 0.05 to show the effect of reduced frequency. Arrows are added to the plots to indicate the direction of the pitching motion in time. The k=0.025 case shows greater unsteadiness only because it represents an average of half as many pitch oscillations.

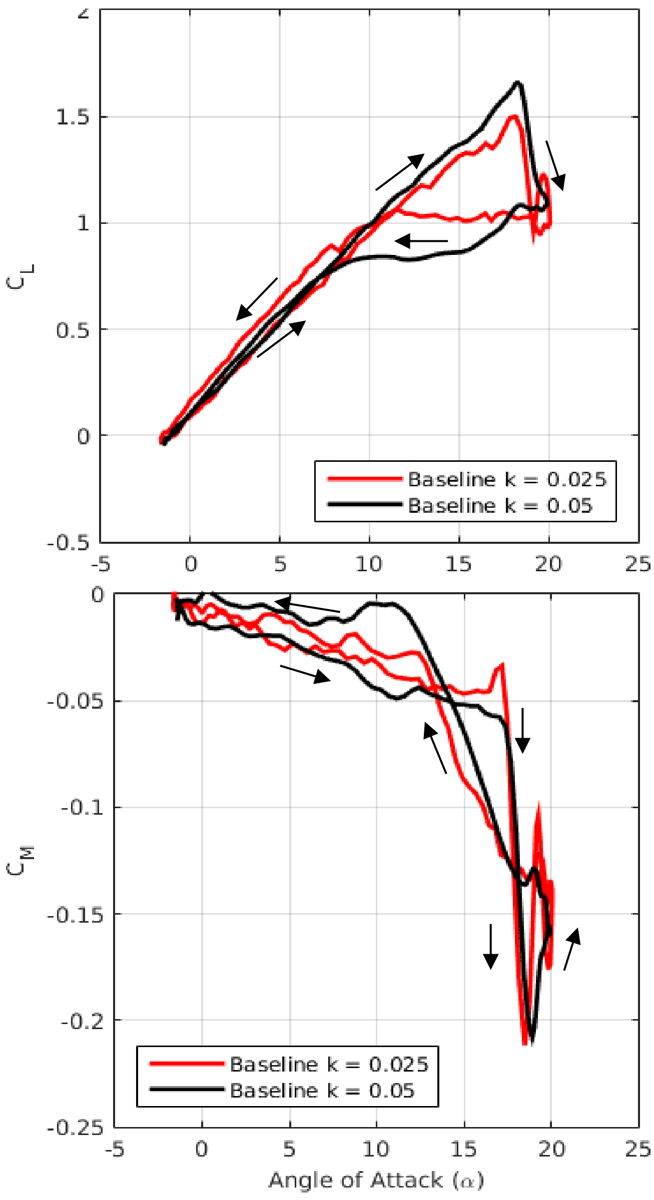

Figure 7: C_L and C_M vs. α for Mach=0.2 and k=0.025 & 0.05. Baseline case with no blowing. (α=9° ±11°). Arrows indicate direction of pitching motion in time.

From Fig. 7 it is clear that the increase in reduced frequency results in larger hysteresis in both c_L and c_M . The lift recovery moves from 12° at k=0.025 to below 8° for k=0.05. The negative damping region in the c_M loop (region of clockwise rotation) also changes with reduced frequency as does the peak negative moment spike.

As the steady flow Mach number is increased from 0.2 to 0.4, the lift slope increases slightly and the stall is earlier and less abrupt (all as expected) with a lower peak c_L (Figs. 8a&b). The moment stall is also less severe and the negative pitching spike is muted somewhat. The results with k and M in Figs. 7 and 8 are consistent with dynamic stall trends documented by numerous researchers.

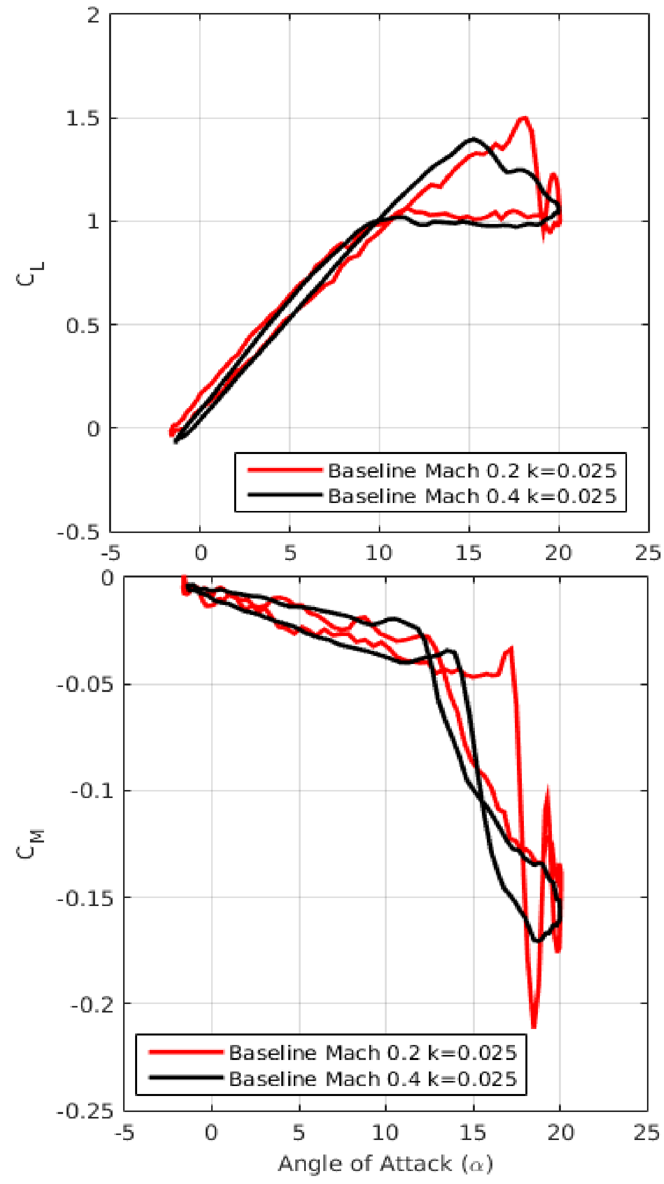

Figure 8: C_L and C_M vs. α for Mach=0.2 & 0.4 and k=0.025. Baseline case with no blowing. (α=9° ±11°)

Synchronized Control, Steady Freestream:

Synchronized VGJ control was studied for a variety of test conditions with a steady freestream before application in an unsteady freestream. Flow control variables include: (1) High or Low pressure (2) actuation initiation (α_{init}) of 17°, 18°, or 19° and (3) actuation duration (α_{on}) of 4.2%, 11.1%, and 16.7% of the pitching period. Figure 9 shows the c_L loop only for α_{init} = 19° and α_{on} = 11.1% at M=0.2 and k=0.05. Data for both the low and high pressure actuation are shown. In this case, and all other cases, the high pressure case was notably superior to the low pressure case. The low pressure actuation did not sustain the lift enhancement during the downstroke following stall and the lift recovery is essentially equivalent to the baseline case (8°). The high pressure actuation case also delays the lift stall slightly (by 1 degree) while the low pressure case does not. Though not shown, the maximum negative c_M (moment spike) is reduced for the high pressure actuation case and the negative damping is slightly lower. Accordingly, all remaining plots will be for the high pressure case only. By way of comparison, Fig. 9 also includes the c_L loop for steady actuation at both the "Peak" and "High" levels introduced in Fig. 6. Already we see that the synchronized actuation is at least as effective as the steady "High Blowing Peak" case, of course with lower net massflow required.

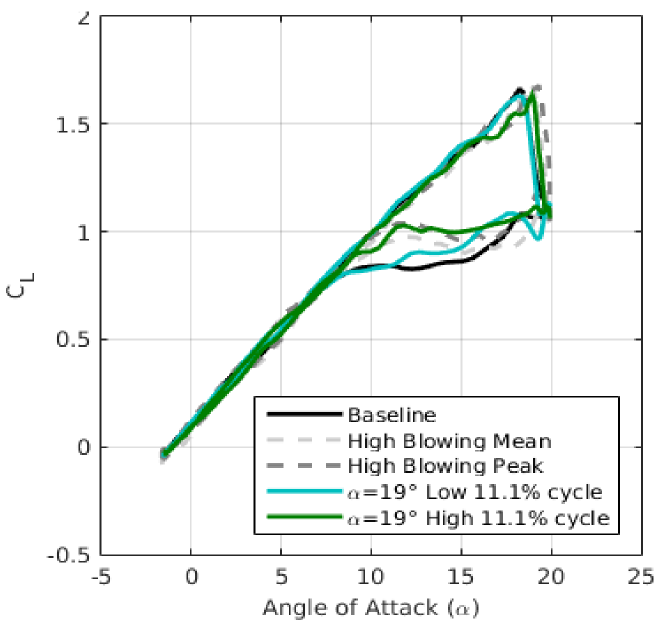

Figure 9: C_L vs. α for Mach=0.2 and k=0.05. Baseline case with no blowing compared to synchronized blowing with α_{init} = 17°, α_{on} = 11.1%, and "High" and "Low" pressure. Steady actuation at "Peak" and "Mean" settings also included. (α=9° ±11°)

The next variable studied was the actuation initiation angle, α_{init}. Figure 10 includes the c_L and c_M hysteresis loops for the case of steady flow at M=0.2 (k=0.05) with α_{init} = 17°, 18°, and 19°. Data are shown for the high pressure setting (as indicated earlier) with the 40° cutout disk (11.1% of the full pitching period). For this case, the 18° and 19° initiation angles yielded very similar results, while the 17° case was definitely inferior. This was generally true for all test conditions and corroborates the findings reported by Matalanis et al. (Ref. 24) given that the baseline stall angle is approximately 18°.

For α_{init} = 18°, lift stall is delayed to a higher angle of attack, whereas pulsing at α_{init} = 19° has a higher average c_L during the downstroke. Due to the later lift stall for α_{init} = 18°, the moment stall is also delayed, reducing the moment spike. At the same time, with α_{init} = 19° the negative damping is nearly eliminated from the c_M loop. Since initiating actuation beyond lift stall misses the opportunity to influence the moment spike, α_{init} values greater than 19° were not attempted in this study.

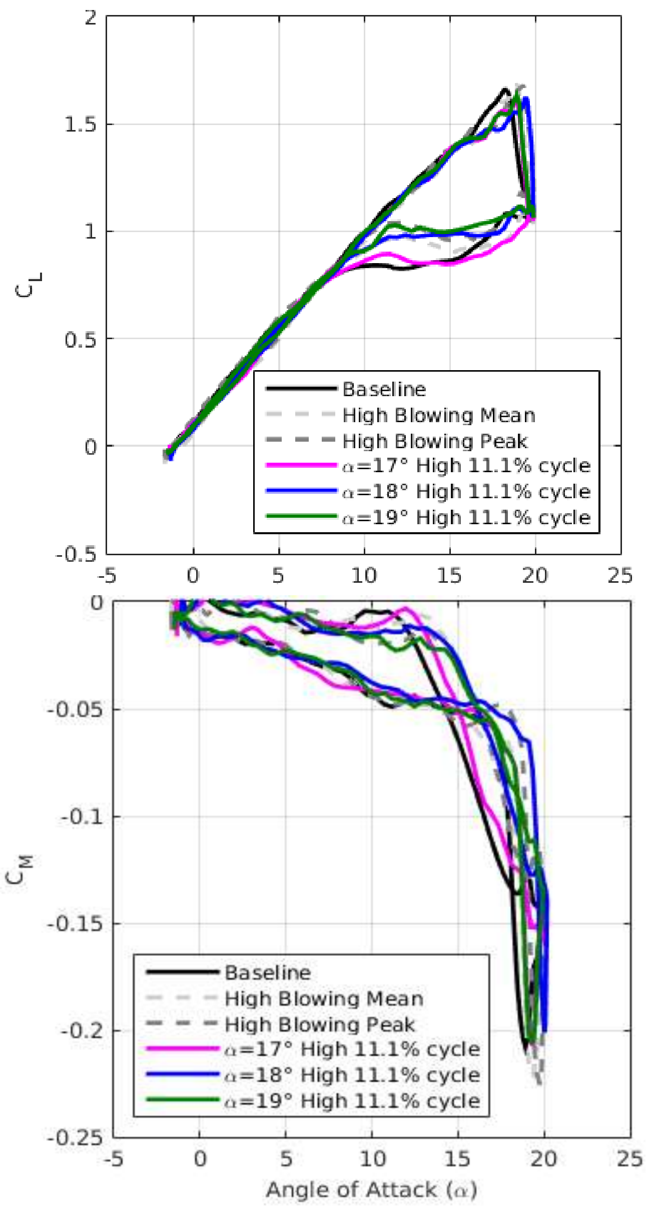

Figure 10: C_L and C_M vs. α for Mach=0.2 and k=0.05. Baseline case with no blowing compared to synchronized blowing with 3 initiation angles, α_{init} = 17°, 18°, & 19° for α_{on} = 11.1%, and "High" pressure. Steady actuation at "Peak" and "Mean" settings also included. (α=9° ±11°).

With the focus now turned to the pulse duration, Fig. 11 includes all 3 cutout disks (4.2%, 11.1%, & 16.7%) with α_{init} = 19° for the same conditions in Fig. 10 (M=0.2, k=0.05, high pressure). Here again, the two longer duration pulses are definitely superior to the 4.2% case. For the longest α_{on} case studied (16.7%), the lift stall is delayed and the recovery c_L has the highest average value. At the same time, the α_{on} = 11.1% case virtually eliminates the negative damping in the c_M loop and has a less severe moment spike compared to the 16.7% case. Since the pulse waveforms differ substantially for the α_{on} = 11.1% and 16.7% cases (as shown in Fig. 6) there is some uncertainty as to which attributes of the pulse waveform are responsible for the improvements at 11.1% and 16.7%: the duration of the peak actuation, the lower level of blowing during the “off” cycle, or the “flat” vs. “double-hump” waveform shape. Further study is clearly warranted with a more precise actuation waveform.

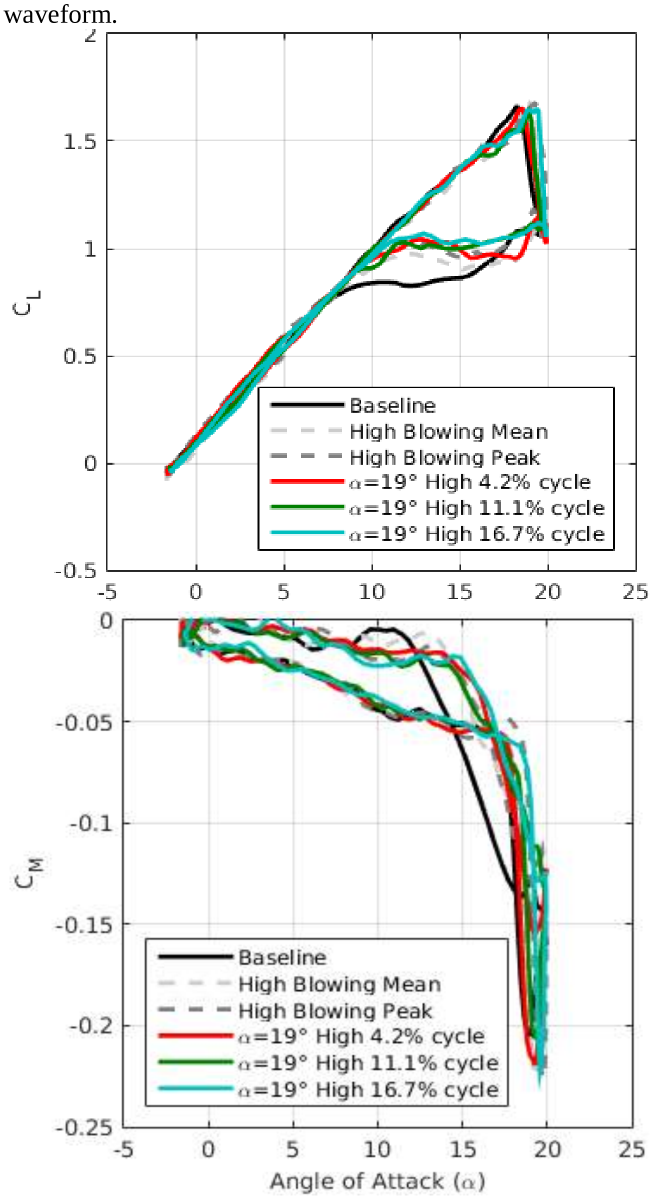

Figure 11: C_L and C_M vs. α for Mach=0.2 and k=0.05. Baseline case with no blowing compared to synchronized blowing with 3 initiation durations, α_{on} = 4.2%, 11.1%, & 16.7% for α_{init} = 19°, and “High” pressure. Steady actuation at “Peak” and “Mean” settings also included. (α=9° ±11°).

Matalanis et al. (Ref 24) found that actuation for longer than 30% of the pitching cycle yielded no significant benefit (and wasted massflow) and Tran et al. only reported 30% actuation in their CFD study. Though no testing was conducted beyond 16.7% in this study, it is not anticipated that prolonged actuation would be beneficial. In fact, it is possible that additional injection could feed into the dynamic stall vortex and strengthen it, exacerbating the unsteady airfoil loads.

To better understand the interaction of the VGJs with the DS vortex it is helpful to look at the unsteady pressure distribution on the suction surface of the airfoil. Figure 12 contains c_P contour plots for 3 cases in an x-ϕ format. Chordwise position is plotted on the x-axis while the y-axis is the phase position in the pitching cycle. Data are shown for the baseline case and both steady and synchronized actuation (α_{init} = 19°) at M=0.2 & k=0.05. In the baseline case, evidence of stall occurs near ϕ = 150° as the suction peak near the leading edge drops off abruptly. The low pressure zone associated with the DS leading edge vortex can then be seen convecting downstream, reaching the trailing edge near ϕ = 170°. There is some evidence of a secondary vortex shed near ϕ = 200° before full lift recovery occurs for ϕ > 240°. With synchronized blowing, the footprint of the DS vortex is not as severe, attenuating earlier during the convection process. Also, the secondary vortex is not apparent and lift recovery is earlier and more stable. While many of the same observations can be made for the steady blowing case (High Blowing Peak), the synchronized actuation is definitely superior. This is all the more remarkable since the synchronized actuation case uses less net massflow.

At the higher Mach number (M=0.4), testing was conducted over a more limited range: α_{on} = 11.1% & 16.7%, α_{init} = 18° & 19° with “High” pressure only. Figure 13 includes the c_L and c_M hysteresis loops for the case of M=0.4 (k=0.025) with α_{init} = 18° and 19°. Data are shown for the high pressure setting with the 40° cutout disk (11.1% of the full pitching period). Many of the features evident at the lower Mach number are evident here as well. Since peak c_L happens earlier at M=0.4 (just past α = 15° vs. 18° at M=0.2), VGJ actuation is initiated during lift stall, which is much more gradual at this Mach number and reduced frequency. Synchronized blowing very nearly matches the performance of the steady “High Blowing Peak” case, which is also shown in Fig. 13. There is very little distinction between the results for actuation at α_{init} = 18° & 19°, the latter case exhibiting a slightly reduced negative damping with an earlier moment (lift) recovery.

Figure 14 shows the c_L and c_M hysteresis loops for the case of M=0.4 (k=0.025) with α_{on} = 11.1% & 16.7%. Data are shown for the high pressure setting with α_{init} = 19°. The only significant difference noted is in the c_M loop, where the added massflow (16.7%) exacerbates the secondary spike during moment stall.

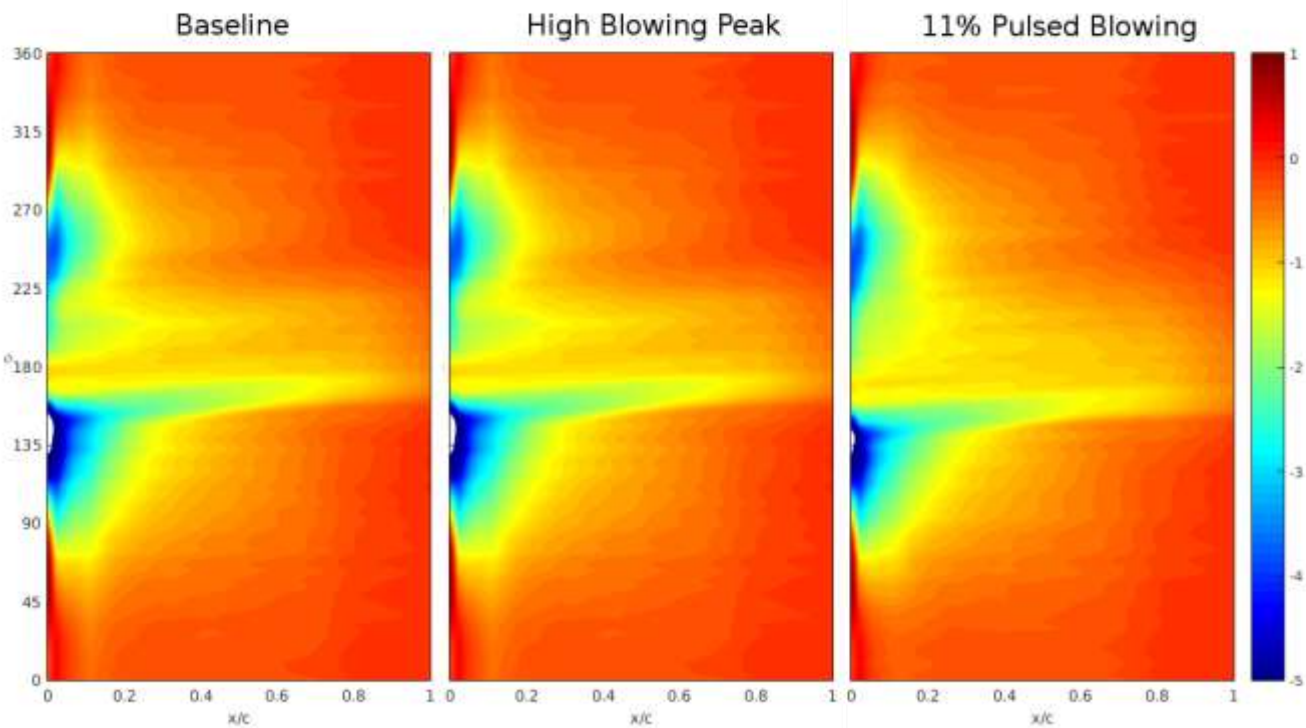

Figure 12: C_P contour plots (x/c vs. ϕ) for Mach=0.2 and k=0.05. Baseline case with no blowing compared to steady blowing at "Peak" pressure and synchronized blowing at α_{on} = 11.1%, α_{init} = 19°, and "High" pressure. (α=9° ±11°).

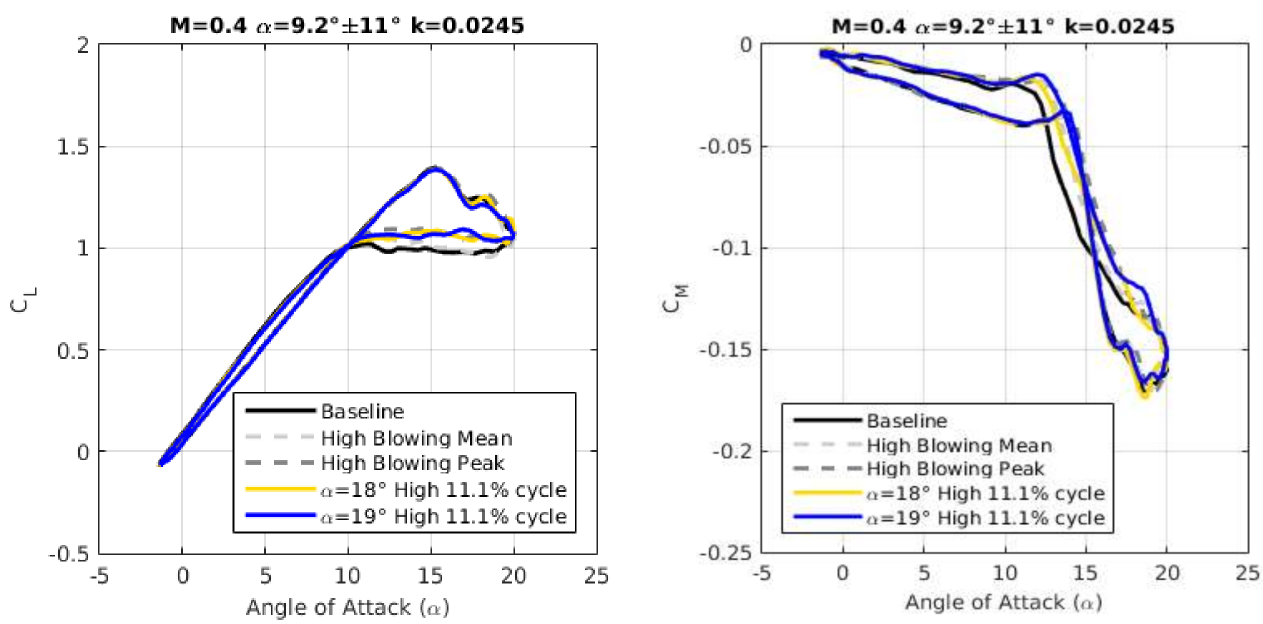

Figure 13: C_L and C_M vs. α for Mach=0.4 and k=0.025. Baseline case with no blowing compared to synchronized blowing with 2 initiation angles, α_{init} = 18° & 19° for α_{on} = 11.1%, and "High" pressure. Steady actuation at "Peak" and "Mean" settings also included. (α=9° ±11°).

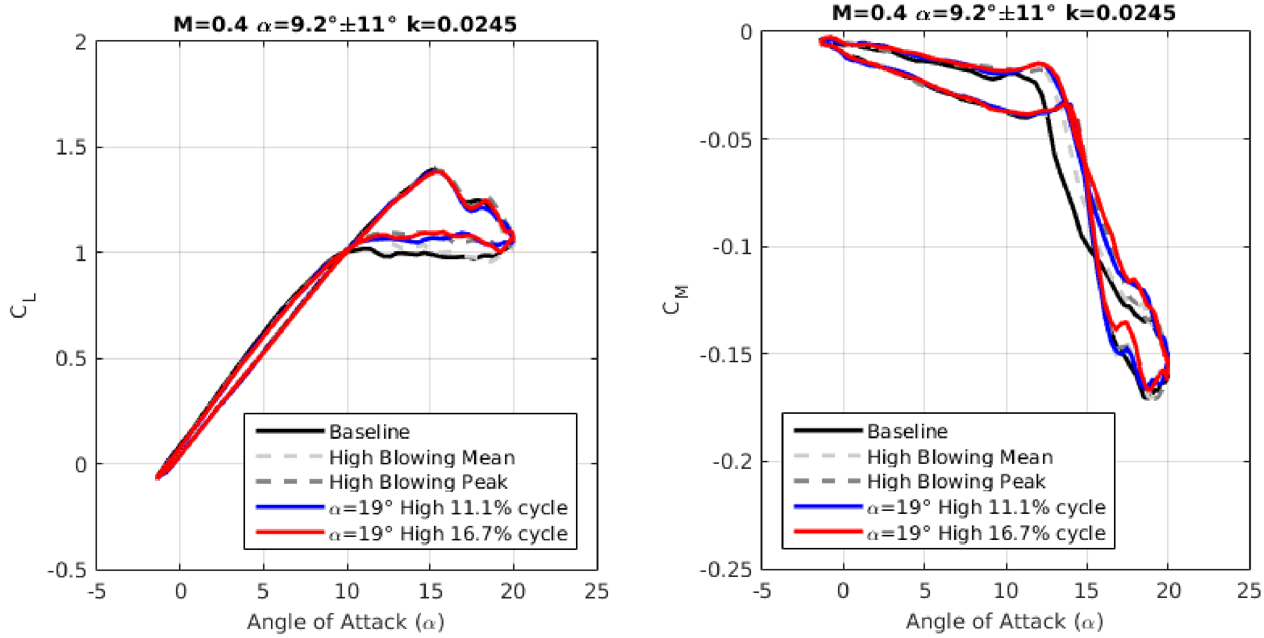

Figure 14: C_L and C_M vs. α for Mach=0.4 and k=0.025. Baseline case with no blowing compared to synchronized blowing with 2 actuation durations, α_{on} = 11.1% & 16.7%, for α_{init} = 19° and "High" pressure. Steady actuation at "Peak" and "Mean" settings also included. (α=9° ±11°).

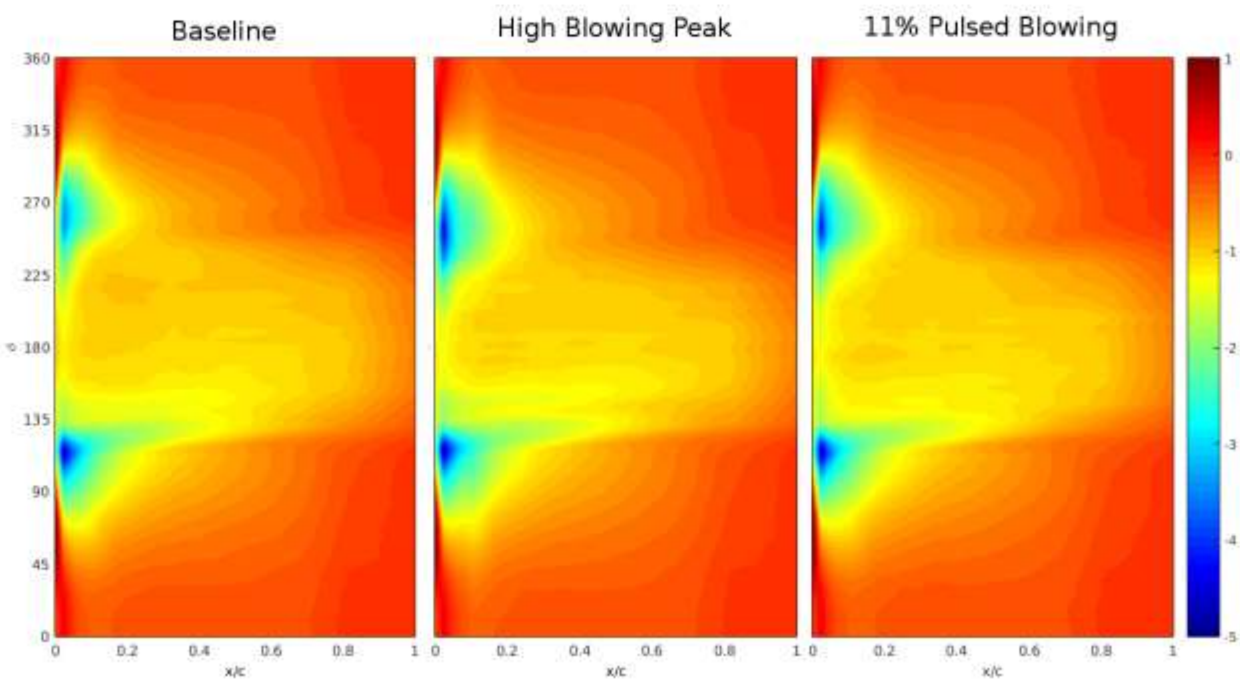

Figure 15: C_P contour plots (x/c vs. ϕ) for Mach=0.4 and k=0.025. Baseline case with no blowing compared to steady blowing at "Peak" pressure and synchronized blowing at α_{on} = 11.1%, α_{init} = 19°, and "High" pressure. (α=9° ±11°).

The pressure coefficient contour maps for M=0.4 and k=0.025 are shown in Fig. 15 for the baseline, steady (peak) blowing, and synchronized blowing cases (α_{on} = 11.1% at α_{init} = 19°). The lift stall phenomenon occurs earlier than in Fig. 12 and is unaffected by the actuation due to the later α_{init}. In fact, the lift stall for all 3 contour maps looks identical, even for the case of steady blowing throughout the entire pitch cycle. Again, the sharp peak of the synchronized blowing case appears to mute the secondary stall event at ϕ = 145°. The lift recovery from 225° < ϕ < 300° is more pronounced and sustained for the 2 actuation cases compared to the baseline c_p. Since the steady (peak) actuation case delivers the same massflow as the maximum value attained by the synchronized blowing (see Fig. 6), it is clear that the impulsive opening of the oscillatory valve creates a dynamic that is singularly beneficial for effective flow control.

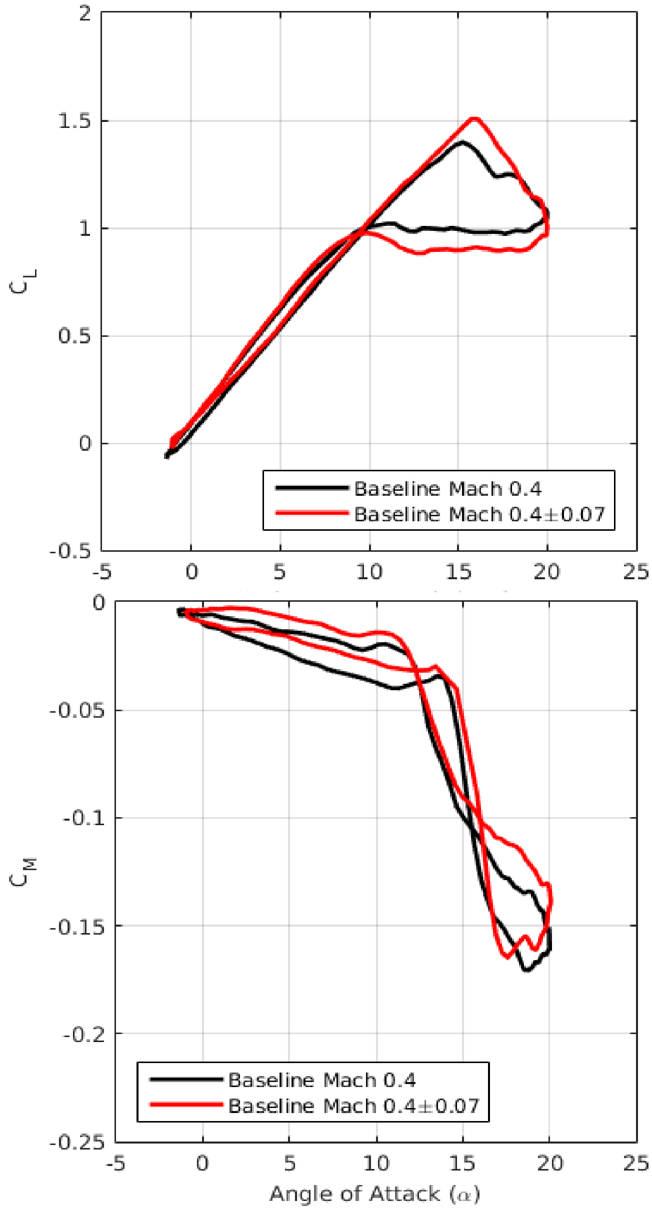

Figure 16: C_L and C_M vs. α for steady M=0.4 vs. oscillating Mach = 0.4±0.07 at k=0.025. Baseline case with no blowing. (α=9° ±11°).

Baseline, No Control, Unsteady Freestream:
Figure 16 shows the uncontrolled pitching airfoil c_L and c_M hysteresis loops for the case of steady M=0.4 vs. oscillating Mach = 0.4±0.07 at k=0.025. For the unsteady freestream case, the Mach oscillation is 180° out of phase with the pitch oscillation such that at the peak α the Mach number is at its minimum value, as would be the case for a helicopter rotor in forward flight (Fig. 17).

As shown previously by Hird et al. (Ref. 12), the decelerating freestream combined with the aggressive pitch up motion exacerbate the hysteresis producing a higher c_L max and a depressed post-stall recovery. The remainder of the c_L loop (the lift slope and the increased lift during the attached part of the pitch down motion) is virtually unchanged. The effect of the freestream deceleration on c_L max is partly obfuscated by the lower freestream velocity in the denominator of the lift coefficient normalization. Figure 17 shows the phase history of angle of attack and Mach number for the unsteady Mach case. The 12.5% drop in M (from the mean value of 0.4 to 0.35 at α = 16°) translates to a 23% drop in dynamic pressure (and thus a commensurate increase in c_L). So, if the physical lift force on the pitching airfoil at c_L max was the same in the steady and unsteady Mach cases, the peak c_L would increase from 1.4 to 1.82 from the normalization alone. The fact that the peak c_L only reaches 1.5 indicates a much weaker suction peak due to the decelerating freestream. Accordingly, the moment spike in the c_M plot is also muted in the oscillating Mach case.

Similarly, in the post-stall recovery during the downstroke from α = 20° to 10°, the unsteady Mach number (and normalizing dynamic pressure) is still below the mean value, which should artificially raise the lift coefficient. Yet, c_L with the oscillating freestream is lower than the steady Mach case during this recovery. Though the freestream Mach is accelerating, the vestiges of the flow deceleration up to α = 20° must continue to have a destabilizing effect on the recovery of the separated boundary layer.

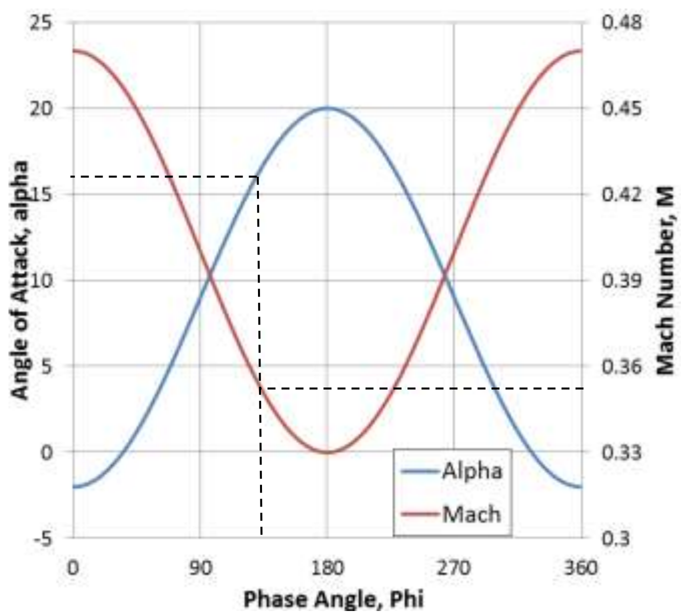

Figure 17: Phase history of α and Mach number for the oscillating Mach = 0.4±0.07 case at k=0.025. Location of max c_L noted with dashed lines.

Synchronized Control, Steady Freestream:
Since the simultaneously oscillating pitch and freestream case is the most challenging to execute, an even more abbreviated test series was conducted in this case: α_{init} = 17°,

18°, & 19° at α_{on} = 11.1% and "High" pressure only. Figure 18 includes the c_L and c_M hysteresis loops for these three cases with Mach = 0.4±0.07 at k=0.025. Many of the features evident in the corresponding steady Mach number case (Fig. 13) are evident here as well. In all 3 cases, VGJ actuation is initiated during lift stall, and thus no effect is obvious until the lift recovery phase on the downstroke. During this time, lift is augmented, the lift performance is recovered earlier, and the negative damping is reduced substantially. There is however very little distinction between the results for different actuator initiation angles; α_{init} = 19° exhibits the smallest negative damping and moment spike while 18° has the best moment (lift) recovery. Though the steady "Peak" and "Mean" blowing cases were not tested in this case, it is anticipated that the synchronized result would be comparable to the steady "Peak" case and superior to the steady "Mean" case, as has been demonstrated repeatedly. Thus, the added freestream dynamic does not impair the ability of synchronized blowing to effectively recover 10-15% of the lift (compared to the baseline) and reduce negative damping by 60-70% in the post-stall regime.

CONCLUSION

Synchronized dynamic stall control with unsteady blowing on a SSC-A09 airfoil was investigated with dynamic pitching motion at steady Mach 0.2 and 0.4 as well as dynamic pitching phase-locked with an oscillating freestream at Mach 0.4±0.07. The Reynolds numbers for the experiments were 1.5M and 2.9M at each Mach number. Flow control variables included: (1) High or Low pressure (2) actuation initiation (α_{init}) of 17°, 18°, or 19° and (3) actuation duration (α_{on}) of 4.2%, 11.1%, and 16.7% of the pitching period. Actuation was found to be most effective when initiated just after lift stall and maintained for at least 11% of the pitching cycle. Blowing beyond 11% provided no appreciable benefit. With actuation, post-stall lift was enhanced, lift recovery occurred sooner, and negative damping was reduced substantially. For select cases, a very modest benefit was seen in the lift stall delay and the moment spike amplitude as well. Pressure contours clearly show that the unsteady nature of the synchronized blowing serves to damp out the secondary stall event and produce a stronger, earlier lift recovery. When compared with steady blowing at the same maximum VGJ amplitude, synchronized blowing at an optimized start time and duration produces equivalent stall suppression while requiring up to 50% less massflow.

Author Contact:
Dr. Jeffrey P. Bons, bons.2@osu.edu
Matthew W. Frankhouser, frankhouser.12@osu.edu
Dr. James W. Gregory, gregory.234@osu.edu

ACKNOWLEDGEMENTS

This work would not have been possible without the assistance of Major Shawn Naigle and Rodrigo Auza Gutierrez. The work was funded by the Army Research Office Short Term Innovative Research (STIR) Program, grant number W911NF-15-1-0207, monitored by Dr. Matthew Munson.

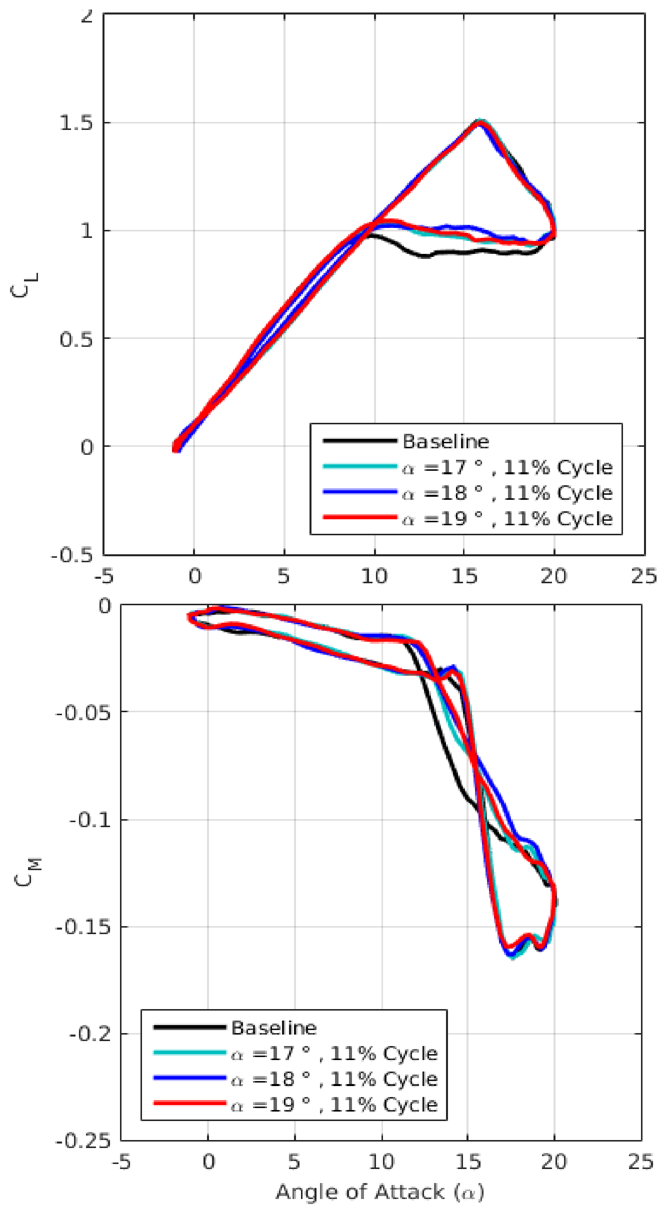

Figure 18: C_L and C_M vs. α for Mach = 0.4±0.07 case at k=0.025. Baseline case with no blowing compared to synchronized blowing with 3 initiation angles, α_{init} = 17°, 18°, & 19° for α_{on} = 11.1%, and "High" pressure. (α=9° ±11°).

REFERENCES

1. McCroskey, W. J., Carr, L. W., and McAlister, K. W., "Dynamic Stall Experiments on Oscillating Airfoils," *AIAA Journal*, Vol. 14, (1), 1976, pp. 57-63.
2. Carr, L. W., "Progress in Analysis and Prediction of Dynamic Stall," *Journal of Aircraft*, Vol. 25, (1), 1988, pp. 6-17.

3. Geissler, W., Dietz, G., and Mai, H., (2005) "Dynamic stall on a supercritical airfoil," Aerospace Science and Technology, Vol. 9, pp. 390-399.
4. Mulleners, K. and Raffel, M., (2013), "Dynamic stall development," Experiments in Fluids, Vol. 54, 1469, doi: 10.1007/s00348-013-1469-7.
5. Raghav, V. and Komerath, N., (2013), "An Exploration of Radial Flow on a Rotating Blade in Retreating Blade Stall," Journal of the American Helicopter Society, Vol. 58, 022005, doi: 10.4050/JAHS.58.022005.
6. Pruski, B.J. and Bowersox, R.D.W., (2013), "Leading-Edge Flow Structure of a Dynamically Pitching NACA 0012 Airfoil," AIAA Journal, Vol. 51, No. 5, pp. 1042-1053.
7. Müller-Vahl, H.F., Nayeri, C.N., Paschereit, C.O., and Greenblatt, D., (2014), "Control of Unsteady Aerodynamic Loads Using Adaptive Blowing," AIAA 2014-2562, 32nd AIAA Applied Aerodynamics Conference, June 16-20, 2014, Atlanta, GA.
8. Ericsson, L. E., (1985) "Is Any Free Flight/Wind Tunnel Equivalence Concept Valid for Unsteady Viscous Flow?," Journal of Aircraft, Vol. 22, No. 10, pp. 915-919.
9. Pierce, G. A., Kunz, D. L., and Malone, J. B., (1978) "The Effect of Varying Freestream Velocity on Airfoil Dynamic Stall Characteristics," Journal of the American Helicopter Society, Vol. 23, No. 2, pp. 27-33.
10. Favier, D., Agnes, A., Barbi, C., and Maresca, C., (1988) "Combined Translation/Pitch Motion: A New Airfoil Dynamic Stall Simulation," Journal of Aircraft, Vol. 25, No. 9, pp. 805-814.
11. Furman, Y., Muller, H.F., and Greenblatt, D., (2013), "Development of a Low-Speed Oscillatory Flow Wind Tunnel", presented at the 51st AIAA ASM conference in Grapevine, TX, Jan 7-10, 2013, #AIAA2013-0505
12. Hird, K., Frankhouser, M.W., Gregory, J.W., and Bons, J.P., "Compressible Dynamic Stall of an SSC-A09 Airfoil Subjected to Coupled Pitch and Freestream Mach Oscillations," Paper AHS 424, American Helicopter Society 70th Annual Forum Proceedings, Montreal, Quebec, Canada, May 20-22, 2014.
13. Chandrasekhara, M. S., Wilder, M. C., and Carr, L. W., (1998) "Competing Mechanisms of Compressible Dynamic Stall," AIAA Journal, Vol. 36, No. 3, pp. 387-393.
14. Carr, L. W., Chandrasekhara, M. S., Wilder, M. C., and Noonan, K. W., (2001) "Effect of Compressibility on Suppression of Dynamic Stall Using a Slotted Airfoil," Journal of Aircraft, Vol. 38, No. 2, pp. 296-309.
15. Martin, P., Wilson, J., Berry, J., Wong, T., Moulton, M., and McVeigh, M., (2008), "Passive control of Compressible Dynamic Stall", 26th AIAA Applied Aerodynamics Conference, Honolulu, HI, August 18-21, 2008, paper #2008-7506.
16. Gerontakas, P. and Lee, T., (2006), "Oscillating Wing Loadings with Trailing-Edge Strips", Journal of Aircraft, Vol. 43, No. 2, Mar-Apr 2006, pp. 428-.
17. Greenblatt, D. and Wygnanski, I., (2001), "Dynamic Stall Control by Periodic Excitation, Part 1: NACA 0015 Parametric Study", Journal of Aircraft, Vol. 38, No. 3, May-June 2001, pp. 430-438.
18. Singh, C., Peake, D.J., Kokkalis, A., Khodagolian, V., Coton, F.N., and Galbraith, R.A.M., (2006), "Control of Rotorcraft Retreating Blade Stall Using Air-Jet Vortex Generators", Journal of Aircraft, Vol. 43, No. 4, Jul-Aug 2006, pp. 1169-1176.
19. Gardner, A.D., Richter, K., Mai, H., and Neuhaus, D., (2014), "Experimental Investigation of Air Jets to Control Shock-Induced Dynamic Stall", Journal of the American Helicopter Society, Vol. 59, 022003, 11 pages.
20. Naigle, S.C., Frankhouser, M.W., Hird, K., Gregory, J.W., and Bons, J.P., "Blowing Flow Control of Dynamic Stall under Coupled Pitch and Freestream Oscillations", presented at the 71st Annual Forum of the American Helicopter Society, May 5-7, 2015, Virginia Beach, Virginia, paper #125.
21. Matalanis, C., Min, B-Y, Bowles, P., Jee, S., Wake, B., Crittenden, T., Woo, G., and Glezer, A., "Combustion-Powered Actuation for Dynamic Stall Suppression Simulations and Low-Mach Experiments," Paper AHS 253, American Helicopter Society 70th Annual Forum Proceedings, Montreal, Quebec, Canada, May 20-22, 2014.
22. Post, M. and Corke, T.C., "Separation Control Using Plasma Actuators: Dynamic Stall Vortex Control on Oscillating Airfoil," *AIAA Journal*, Vol. 44, (12), 2006, pp. 3125-3135.
23. Tran, S.A., Fisher, A.E., Corson, D., and Sahni, O., "Dynamic Stall Alleviation for an SC1095 Airfoil using Synthetic Jet Actuation," presented at the 2015 AIAA SciTech conference in Kissimmee, FL, 5-9, January 2015. AIAA-2015-1038.
24. Matalanis, C., Bowles, P., Lorber, P., Crittenden, T., Glezer, A., Schaeffler, N., Min, B-Y, Jee, S., Kuczek, A., and Wake, B., "High Speed Experiments on Combustion-Powered Actuation for Dynamic Stall Suppression," Paper AHS 160, American Helicopter Society 72nd Annual Forum Proceedings, West Palm Beach, FL, May 17-19, 2016.
25. Gompertz, K., Jensen, C., Kumar, P., Peng, D., Gregory, J. W., and Bons, J. P., "Modification of Transonic Blowdown Wind Tunnel to Produce Oscillating Freestream Mach Number," *AIAA Journal*, Vol. 49, (11), 2011, pp. 2555–2563.
26. Bergh, H. and Tijdeman, H., "Theoretical and Experimental Results for the Dynamic Response of Pressure Measuring Systems," Technical Report TRF.238, Amsterdam Nationaal Luchtvaarlaboratorium (National Aeronautical and Astronautical Research Institute), 1965.
27. Lorber, P.F. and Carter, F.O., "Unsteady Stall Penetration Experiments at High Reynolds Number", AFOSR Technical Report 87-1202, DTIC Document ADA186120, April 1987.
28. Coleman, H. W. and Steele, W. G., *Experimentation and Uncertainty Analysis for Engineers*, 3rd ed., John Wiley & Sons, Inc, New York, NY, 2009.